Reprinted from JOURNAL OF ATMOSPHERIC AND OCEANIC TECHNOLOGY, Vol. 8, No. 5, October 1991
American Meteorological Society

A Simplified Wind Vector Algorithm for Satellite Scatterometers

FRANK J. WENTZ

Remote Sensing Systems, Santa Rosa, California

11 November 1990 and 6 March 1991

ABSTRACT

We derive a simplified algorithm for retrieving wind vectors from microwave scatterometer observations. The azimuthal dependence of the sea surface radar cross section is modeled by a double-cosine function, rather than the traditional second-order cosine expansion. The algorithm is tested using the aircraft scatterometer observations obtained during the AAFE–RADSCAT Experiment in 1975 and 1976. There is little difference between the performance of the simplified algorithm and the more involved least-squares searching algorithm.

The AAFE–RADSCAT aircraft observations are sampled so as to simulate the three-look satellite scatterometer NSCAT that will be launched on the Japanese Advanced Earth Observing Satellite (ADEOS). The results of the retrievals indicate that it is probably not possible to uniquely determine the wind direction using just NSCAT observations because of a 180° ambiguity. However, if forecast models can predict the wind direction to an accuracy of ±90°, thereby eliminating the ambiguity, then the results indicate that NSCAT can determine the wind direction to an accuracy of about ±20°. Better performance is obtained when the three observations are the same polarization (either *v*-pol or *h*-pol), as compared to using a mix of *v*-pol and *h*-pol observations.

1. Introduction

Over the world's oceans and seas, the satellite microwave scatterometer has the capability of sensing the near-surface wind speed and direction. The Seasat scatterometer (SASS), launched in 1978, measured the wind speed to better than 2 m s^{-1} (Jones et al. 1979; Jones et al. 1982). The capability to sense wind direction was partially verified, albeit the direction could not be uniquely determined due to the existence of multiple solutions in the retrieval equations.

Scatterometers scheduled for launching in the 1990s will have an additional antenna (three azimuth looks rather than the two-look configuration used by SASS). The purpose of the third antenna is to reduce the number of multiple solutions. These future scatterometers are the NASA scatterometer (NSCAT) to be launched on the Japanese Advanced Earth Observing Satellite (ADEOS); the scatterometer to be launched on the European Remote Sensing Satellite (*ERS-1*); and NASA's Earth Observing System (EOS) scatterometer.

In this paper, we introduce a new retrieval algorithm for processing scatterometer data. The algorithm is considerably simpler than previous algorithms that search wind vector space for least-squares solutions, such as that originally developed by Wentz et al. (1982). The algorithm is used to reprocess the 3-month SASS dataset. The performance of the algorithm for future three-look scatterometers is tested by using aircraft measurements taken by the RADSCAT scatterometer during the Advanced Applications Flight Experiment (AAFE) conducted by NASA Langley Research Center (Jones et al. 1977). These observations are sampled so as to correspond to the NSCAT azimuth angles.

In the past, computer simulated data have been used to evaluate the performance of three-look scatterometers (Wentz 1979; Grantham et al. 1982; Chi and Li 1988). The simulations herein are intended to complement these earlier studies. As compared to the simulated data, the aircraft data may, in some ways, be more representative of the actual observations that will be obtained by NSCAT.

2. Azimuth-angle dependence of the NRCS

The AAFE–RADSCAT aircraft experiment (Jones et al. 1977; Jones and Schroeder 1978) revealed that the radar return from the sea surface was strongly modulated by the wind direction for incidence angles of 20° and greater. The radar backscattered power is measured in terms of the normalized radar cross section (NRCS), which is denoted by $\sigma°$. The NRCS in the upwind and downwind directions was observed to be substantially larger than the crosswind observations. In addition, the upwind $\sigma°$ was somewhat higher than the downwind $\sigma°$, particularly for horizontal polarization at high incidence angles. These results were obtained by flying the aircraft in circles such that the azimuth angle ϕ_0 of the scatterometer observations varied

Corresponding author address: Dr. Frank J. Wentz, Remote Sensing Systems, 1101 College Ave. Suite 220, Santa Rosa, CA 95404.

from 0° to 360°, while the incidence angle remained constant. A good approximation for the azimuth-angle dependence was found to be

$$\sigma^\circ = A_0 + A_1 \cos\phi + A_2 \cos 2\phi \qquad (1)$$

where ϕ represents the azimuth look angle relative to the azimuth angle of the wind direction ϕ_w, i.e., $\phi = \phi_0 - \phi_w$. Upwind, crosswind, and downwind observations are represented by $\phi = 0°$, $\pm 90°$, and $180°$, respectively. A variation to (1) that is also a good approximation to the aircraft data is

$$\log\sigma^\circ = A_0 + A_1 \cos\phi + A_2 \cos 2\phi. \qquad (2)$$

The A coefficients are implicit functions of polarization ϵ, incidence angle θ_i, and wind speed W. The A_1 coefficient is a measure of the upwind–downwind difference, and the A_2 coefficient is a measure of the along-wind–crosswind difference. This relationship was used by Wentz et al. (1984; 1986) to model the NRCS observations that came from the Seasat scatterometer SASS, and expressions were derived that gave the A coefficients as functions of ϵ, θ_i, and W.

The dependence of the NRCS on azimuth angle can be modeled by another expression, which we call the double-cosine function,

$$\sigma^\circ = A_0 + \gamma(\phi)A_1 + [A_2 + \gamma(\phi)A_1] \cos 2\phi \qquad (3)$$

$$\gamma(\phi) = +0.5, \text{ when } -90° < \phi < 90° \qquad (4a)$$

$$\gamma(\phi) = -0.5, \text{ otherwise.} \qquad (4b)$$

This expression is two cosines with different amplitudes splined together at $-90°$ and $90°$. Equation (3) is identical to (1) for $\phi = 0°$, $90°$, $180°$, and $270°$ and is continuous to the first derivative of ϕ. The primary difference between (1) and (3) is that the minima of (3) occur exactly at $90°$ and $180°$, while the minima of (1) are displaced from the crosswind direction (except for special case of $A_1 = 0$). Our objective in introducing this new azimuthal form for σ° is to simplify the retrieval problem, as is discussed in the next section. Another possible model for the NRCS analogous to (2) is

$$\log\sigma^\circ = A_0 + \gamma(\phi)A_1 + [A_2 + \gamma(\phi)A_1] \cos 2\phi. \qquad (5)$$

An analysis is done to determine how well (1), (2), (3), and (5) fit the AAFE–RADSCAT observations. For each circle flight, values for A_0, A_1, and A_2 are found to best match the aircraft scatterometer data in a least-squares sense. Given these three derived coefficients, the following after-the-fit rms difference is computed:

$$\delta = 10\langle[\log(\sigma^\circ_{\text{mea}}/\sigma^\circ_{\text{mod}})]^2\rangle^{1/2}, \qquad (6)$$

where $\langle\ \rangle$ denotes an average over all observations in all circle datasets (36 azimuth angles times 64 circles). The term $\sigma^\circ_{\text{mea}}$ is the AAFE–RADSCAT observation and $\sigma^\circ_{\text{mod}}$ is the value of the NRCS coming from one of the previous expressions using the coefficients derived from the least-squares fit. There is little difference between the quality of fit for the four expressions. The values of δ for expressions (1), (2), (3), and (5) are 0.46, 0.44, 0.43, and 0.47 dB, respectively. We expect that this variability is primarily due to microscale variations in the surface wind field. As compared to satellite observations, the signal to noise for RADSCAT is large, and hence the variability of σ° due to instrument noise is considerably less than 0.5 dB.

Figures 1 and 2 show an example of a circle dataset for horizontal and vertical polarizations, respectively. The NRCS in decibels (i.e., $10\log\sigma^\circ$) is plotted versus the relative azimuth look angle ϕ. The wind speed for this circle flight is approximately 13 m s^{-1}, and the incidence angle is 40°. The symbols "O" correspond to the aircraft measurements. The model calculations corresponding to expressions (1), (2), (3), and (5) are shown by the large-dashed curve, the small-dashed curve, the solid curve, and the dotted curve, respectively. As can be seen, the differences among the different models are not that significant. This is particularly true for vertical polarization because of the small upwind–downwind asymmetry. When there is no upwind–downwind asymmetry, models (1) and (3) are identical, and models (2) and (5) are also identical.

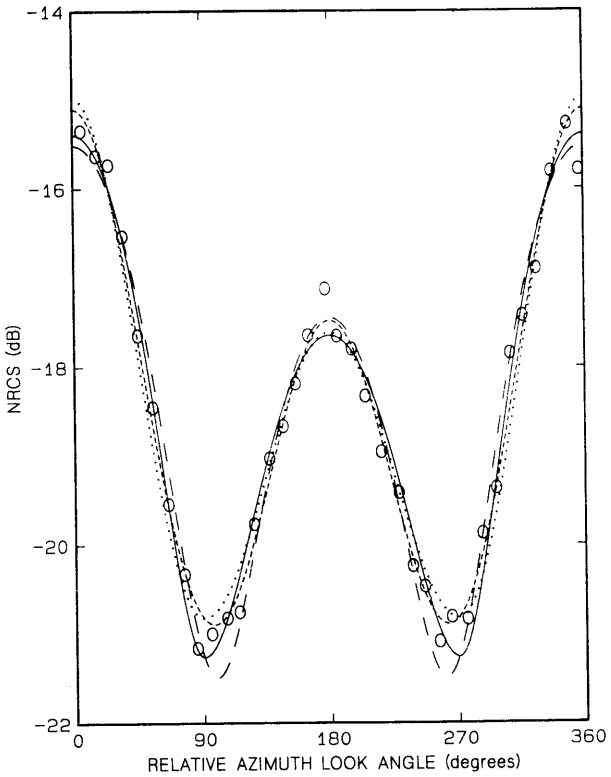

FIG. 1. An example of the NRCS azimuthal dependence for horizontal polarization. The symbol "O" shows the aircraft measurements. The large-dashed, small-dashed, solid, and dotted curves show four different models for the azimuthal dependence.

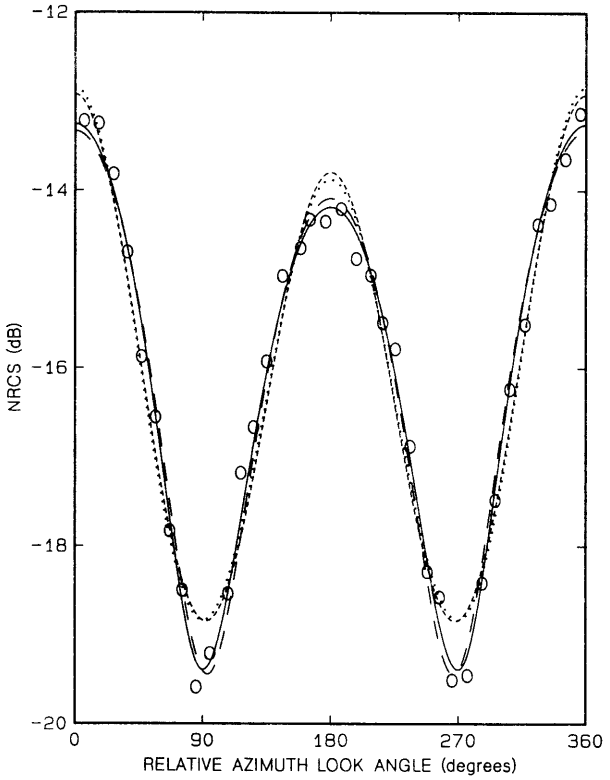

FIG. 2. An example of the NRCS azimuthal dependence for vertical polarization. The symbol "*O*" shows the aircraft measurements. The large-dashed, small-dashed, solid, and dotted curves show four different models for the azimuthal dependence.

With respect to the location of the NRCS maxima and minima, the traditional harmonic-expansion model and the double-cosine model are equally restrictive. Both models require that the maxima occur at 0° and 180°. The harmonic-expansion model places the minima at 90° + $\Delta\phi$ and 270° − $\Delta\phi$, where $\Delta\phi$ depends on the values of A_1 and A_2 and is typically about 5°. The minima of the double-cosine model are exactly at 90° and 270°. Most of the circle datasets show the minima near 90° and 270°, but the data variability precludes determining which model "best" represents the data. In some cases, the observed NRCS azimuthal dependence does not agree with either model, with the minima being shifted by as much as 45° from their typical 90° and 270° locations (Colton 1989). This discrepancy is probably due to a confused sea state. The treatment of these anomalous cases poses a very difficult problem for scatterometry.

In view of the variability in the observed NRCS azimuthal dependence, the differences among the four models does not seem significant, and henceforth (3) will be used to represent the azimuth angle dependence because it simplifies the retrieval problem. However, it is recognized that this conclusion is based on a limited dataset and that additional analyses of other aircraft data may determine a better model. If this occurs, the algorithm presented herein will need to be modified. If the change in the model is not too large, the simplified algorithm could still be used to obtain a "first guess" for the wind vector solutions, which could then be perturbed to account for the change in the azimuthal dependence.

3. Wind vector retrieval from two orthogonal observations

The Seasat scatterometer and the scatterometers planned for future missions such as *ERS-1*, ADEOS, and EOS all have a forward and an aft antenna that observe the ocean surface from orthogonal directions. In addition, the future scatterometers have a third antenna looking between the forward and aft antennas. The purpose of the third antenna is to eliminate some of the multiple solutions that occur when inverting the set of NRCS equations. These multiple solutions are called ambiguities. (In the Seasat literature, they are sometimes referred to as "aliases.") The utility of the third antenna in reducing the number of ambiguities is discussed in the next section.

To begin the formulation of the retrieval algorithm, let $\langle\sigma^\circ\rangle_1$ and $\langle\sigma^\circ\rangle_2$ denote the average value of the forward and aft NRCS, where the average is over an area on the ocean surface. Typically, the areal resolution for the satellite scatterometers is between 25 and 100 km. This average is then given by

$$\langle\sigma^\circ\rangle_i = \langle A_0\rangle_i + \gamma(\phi_i)\langle A_1\rangle_i + [\langle A_2\rangle_i + \gamma(\phi_i)\langle A_1\rangle_i]\cos 2\phi_i \quad (7)$$

where subscript i denotes the antenna ($i = 1$ or 2) and $\langle\ \rangle_i$ denotes an average over all observations within the specified resolution cell. The azimuth observation angle ϕ_{oi} is essentially constant over the resolution cell, and it has been assumed that the wind direction ϕ_w is also constant over the cell. Hence the terms just involving $\phi_i = \phi_{oi} - \phi_w$ can be factored from the averages. The two measurements are orthogonal such that

$$\phi_2 = \phi_1 + 90^\circ. \quad (8)$$

Equation (7) can be rewritten as

$$\langle\sigma^\circ\rangle_i = P_{ij} + Q_{ij}\cos 2\phi_i \quad (9)$$

$$P_{ij} = \langle A_0\rangle_i + \gamma_{ij}\langle A_1\rangle_i \quad (10)$$

$$Q_{ij} = \langle A_2\rangle_i + \gamma_{ij}\langle A_1\rangle_i. \quad (11)$$

The function $\gamma(\phi_i)$ is now denoted by γ_{ij}, where the subscript j denotes one of four possible cases given in Table 1.

By combining the two equations represented by (9) for the forward and aft antennas, the cosine term can be eliminated, resulting in the following expression:

TABLE 1. Four possible cases for relative azimuth angle.

Subscript j	Range of ϕ_1	γ_{1j}	γ_{2j}
1	0°–90°	0.5	−0.5
2	90°–180°	−0.5	−0.5
3	180°–270°	−0.5	0.5
4	270°–360°	0.5	0.5

$$f(W) \equiv Q_{1j}(\langle \sigma_2^\circ \rangle - P_{2j}) + Q_{2j}(\langle \sigma_1^\circ \rangle - P_{1j}) = 0. \quad (12)$$

The P and Q coefficients are functions of polarization, incidence angle, wind speed, and case number j. The polarization and incidence angle are known, and for each case a wind speed is easily found by Newton's method. For example, let W_a be the first guess. Then the second guess is given by

$$W_b = W_a - f(W_a)(df/dW)^{-1}, \quad (13)$$

where df/dW is the derivative of $f(W)$ with respect to W evaluated at W_a. A few iterations are required to converge to 0.1% in wind speed. A wind speed is found for each of the four possible azimuth-angle cases. These solutions are denoted by W_j. This wind speed is substituted into (9), and a $\cos 2\phi_1$, denoted by X_j, is found for each case,

$$X_j \equiv \cos 2\phi_1 = (\langle \sigma^\circ \rangle_1 - \langle \sigma^\circ \rangle_2 - P_{1j} + P_{2j}) \times (Q_{1j} + Q_{2j})^{-1}. \quad (14)$$

Henceforth, the subscript for ϕ will denote the azimuth case (i.e., j) rather than the antenna number, and it will be understood that ϕ refers to the forward antenna. The arccosine function is then used to find a value of ϕ for each case. Since each case restricts the range of ϕ to 90°, there is no problem with the multiple values given by the arccosine operation. The values of ϕ for the four cases are given by

$$\phi_1 = \arccos(X_1)/2 \quad (15a)$$

$$\phi_2 = 180^\circ - \arccos(X_2)/2 \quad (15b)$$

$$\phi_3 = 180^\circ + \arccos(X_3)/2 \quad (15c)$$

$$\phi_4 = 360^\circ - \arccos(X_4)/2, \quad (15d)$$

and the ambiguity wind directions are

$$\phi_{wj} = \phi_0 - \phi_j. \quad (16)$$

In analyzing the wind vector solutions, we first note that when there is no upwind–downwind difference in the NRCS, i.e., $A_1 = 0$, then Eqs. (12) and (14) are no longer dependent on the azimuth angle case. Hence the values found for W_j and X_j will be the same for $j = 1$–4. The previous equations then become

$$\phi_1 = \arccos(X)/2 \quad (17a)$$

$$\phi_2 = 180^\circ - \phi_1 \quad (17b)$$

$$\phi_3 = -\phi_2 \quad (17c)$$

$$\phi_4 = -\phi_1. \quad (17d)$$

As X goes from 1 (wind aligned with forward antenna) to −1 (wind orthogonal to forward antenna), ϕ_1 rotates from 0° to 90°. The other three possible directions rotate symmetrically with ϕ_1. There are always four distinct ambiguities of ϕ, with the following exception. When X equals either 1 or −1, a degenerate case occurs for which the four ambiguities merged into two ambiguities separated by 180°. Note that if we assume a perfect model and noise-free observations, X will always lie within the −1 to 1 range.

An upwind–downwind difference somewhat complicates the solution, but each ϕ ambiguity will still lie in a distinct quadrant, and the maximum number of ambiguities is still 4. When the wind direction is close to the direction of either the forward or aft antenna, the upwind–downwind difference can produce situations in which there are only 1, 2, or 3 ambiguities. These cases are distinguished by the fact that one or more of the values for X_j lie outside the range of −1 to 1, which indicates there is no solution for the quadrant. However, at least one of the X_j will lie within the −1 to 1 range assuming a perfect model and noise-free observations.

As an example, let the upwind–downwind difference be 1 dB, and let the upwind–crosswind difference be 6 dB. The downwind–crosswind difference will then be 5 dB. If the forward antenna observation is 6 dB higher than the aft antenna observation, then this indicates that the forward antenna must be looking in the upwind direction, i.e., $\phi = 0°$. For this case, X_1 and X_4 will equal 1, while X_2 and X_3 will lie outside the −1 to 1 range.

In reality, errors in the σ° model and observations make it difficult to eliminate ambiguities based on $|X_j|$ exceeding 1. When the upwind–downwind difference is of the order of (or less than) the modeling-measurement error, then it is probably best to assume an ambiguity exists for each quadrant. This is the case for v-pol observations. The likely cause of $|X_j|$ exceeding unity is the modeling-measurement error rather than there being no solution for the quadrant. To avoid excluding a possible solution, X_j can be reset to either −1 or 1, and a value for ϕ can be found for the quadrant. This is the approach used for the analyses that follow.

The h-pol observations at the higher incidence angles show a significant upwind–downwind difference, and the possibility exists that ambiguities can be removed based on the degree to which $|X_j|$ exceeds unity. However, the observed upwind–downwind difference shows considerable variation from one circle flight to another, i.e., there is a large modeling error. It is unclear if partial ambiguity removal based on $|X_j|$ exceeding unity would be successful for the case of two orthogonal h-pol observations.

Note that the wind speed values for the different ambiguities are similar, typically varying by only 2% for the v-pol observations and 6% for the h-pol observations. Thus, the ambiguity problem is of minor consequence to the wind speed retrieval. An accurate wind speed can be obtained by simply setting the A_1 coefficient to zero.

For this case of a two-orthogonal-look scatterometer, the least-squares searching algorithms will find the same solutions as given by (13) and (15). That is to say, there is a unique set of solutions that both methods find. However, the simplified algorithm is a more efficient way of finding these solutions. When a third azimuth look is considered, the problem becomes overdetermined, and the solution depends on how the three observations are weighted, as is discussed in the next section.

The simplified algorithm has been used to reprocess the 3-month SASS dataset. In doing this, the SASS-II NRCS model derived by Wentz et al. (1984, 1986) is used to specify the A coefficients. This SASS-II wind vector dataset is currently being evaluated by a number of investigators.

4. Ambiguity removal with a three-look scatterometer

A third antenna provides the means to eliminate some of the wind direction ambiguities given by (15). A simple way to accomplish this is to determine which ambiguities produce σ° values that do not agree with the observation made by the third antenna. Let $\mathbf{W}_j$ denote the four wind vector ambiguities derived from the forward and aft NRCS observations, and let $F_i(\mathbf{W}_j)$ denote the NRCS model [i.e., Eq. (7)], where subscript $i = 1$, 2, and 3, corresponding to the forward, aft, and middle antenna, respectively. The measured NRCS value for the forward, aft, and middle antennas are denoted by σ_1°, σ_2°, and σ_3°, respectively (the area average $\langle\ \rangle$ brackets are now implicit). Since $\mathbf{W}_j$ is computed from σ_1° and σ_2°, the following conditions hold for those ambiguities having $|X_j| \leq 1$.
Here

$$\Delta_{1j} \equiv \log[\sigma_1^\circ / F_1(\mathbf{W}_j)] = 0 \qquad (18a)$$

$$\Delta_{2j} \equiv \log[\sigma_2^\circ / F_2(\mathbf{W}_j)] = 0. \qquad (18b)$$

The observation versus model NRCS difference Δ_{3j} for the middle antenna indicates which ambiguities can be eliminated,

$$\Delta_{3j} \equiv \log[\sigma_3^\circ / F_3(\mathbf{W}_j)]. \qquad (19)$$

The number of j ambiguities is 4 except for the degenerate case of the wind blowing exactly in the direction of either the forward or aft antenna, for which j is 1 or 2.

Assuming for now that there is no observation or modeling error, only one of the Δ_{3j} is zero when $A_1 \neq 0$, and the true solution is uniquely determined. This assertion that $A_1 \neq 0$ results in a unique solution is based on the results of many numerical exercises, rather than on an analytical proof. There may be special cases for which multiple solutions exist even when there is an upwind–downwind difference, but none has been found.

When the upwind–downwind difference is zero (i.e., $A_1 = 0$), it can be shown that $\Delta_{31} = \Delta_{33}$ and $\Delta_{32} = \Delta_{34}$, with one pair being zero and the other pair being nonzero. The true solution will be one of the two ambiguities for which Δ_{3j} is zero. In other words, when $A_1 = 0$, a middle antenna reduces the number of ambiguities to two solutions separated by 180°. The 180° ambiguity problem is a fundamental limitation that cannot be resolved if the NRCS simply varies as the $\cos 2\phi$, no matter how many azimuthal observations are made.

In reality, modeling and measurement errors result in none of the Δ_{3j} being exactly zero, and the ambiguity selection becomes a statistical problem. Those ambiguities with small absolute values of Δ_{3j} are more likely to be the true solution than those with larger values. The ambiguity can be ranked according to the value of $|\Delta_{3j}|$, or relative probabilities can be assigned based on the ratio of $|\Delta_{3j}|$ to the expected variation due to modeling and measurement errors. The major limitation in developing statistical procedures for ambiguity removal is our lack of knowledge of the error statistics of the model. In what follows, we outline an approach to the ambiguity selection problem that we think commensurates with our limited knowledge of the model error statistics.

To begin with, we note that Δ_{1j} and Δ_{2j} will be zero, even in the presence of errors, because the wind vector ambiguities $\mathbf{W}_j$ are found by fitting the model to σ_1° and σ_2°. The one exception is when the cosine term X_j lies outside the -1 to 1 range. In this case, no wind vector could be found for the quadrant under consideration that perfectly fits the model to the observations. Hence, Δ_{1j} and Δ_{2j} are not 0, and the degree of this mismatch should be considered in ranking ambiguities. In view of this, Δ_{1j} and Δ_{2j} are included along with Δ_{3j} in determining the quality of fit, and the following quantity is used for ranking the ambiguities:

$$S_j = [\sum (\Delta_{ij})^2]^{1/2}, \qquad (20)$$

where the summation is over $i = 1$–3. The four ambiguities are ranked in the order of ascending values of S_j. The highest-ranked ambiguity (i.e., most likely) is the one that has the smallest S_j.

We note that, in general, the S_j given by the preceding procedure is not necessarily minimized. That is to say, there can (and usually does) exist another wind vector $\mathbf{W}_j'$ in the neighborhood of $\mathbf{W}_j$, which will give a somewhat smaller σ° residual. Wind vector $\mathbf{W}_j'$ can be found by computing S_j on a fine wind vector space grid and thereby locating minima. This searching procedure was

first introduced by Wentz et al. (1982), and since then various perturbations on the technique have been tested (Chi and Li 1988). In these variations, different forms for the residual Δ_{ij} are used, including the original form given by (18) and the form $(\sigma^\circ - F)/V$, where V is some assumed rms variation between the model and the observations.

The obvious question is which procedure and which form of Δ_{ij} is "best." Under error-free conditions, all procedures will give identical results. Thus, it is the statistics of the model and measurement errors that produce differences among the various techniques. If, for example, the errors were Gaussian and uncorrelated (i.e., $\sigma^\circ - F$ is normally distributed) and if we knew the standard deviation V, then the optimum procedure would be to find the S_j minima assuming $\Delta_{ij} = (\sigma^\circ - F)/V$. In reality, we expect the model error to be non-Gaussian and correlated. For NSCAT, the model error for the forward and middle antennas, which are separated by only 20°, may be very correlated. If a strong correlation exists, then it would be incorrect to give equal weight to all three observations. The choice of an optimum ambiguity selection procedure will remain unclear until more is known about the error statistics.

Although the simple procedure previously outlined is certainly not optimum, we suspect that the differences between it and more elaborate search procedures will not be that significant when put in the proper perspective with the uncertainties in the model. The next section examines this question further.

5. Algorithm test using aircraft observations

The performance of the simplified wind vector retrieval algorithm is tested using the AAFE–RADSCAT aircraft observations. The AAFE–RADSCAT scatterometer operated at 13.9 GHz and was mounted on the open cargo ramp of a C-130 aircraft. The data from missions 306, 318, and 335 are used. Mission 306 (April 1975) and mission 335 (January 1976) were flown a few hundred kilometers off the Virginia coast. Mission 318 (September 1975) was part of the JONSWAP experiment and was flown over the North Sea. The aircraft was flown in circles maintaining a constant banking angle, and the NRCS measurements were averaged into 36 10° azimuth-angle bins. A total of 32 *h*-pol circle datasets and 32 *v*-pol circle datasets were obtained. The incidence angle for these various circle flights ranged from 20° to 62°. The AAFE–RADSCAT data archive is described by Schroeder and Mitchell (1983).

For each circle dataset, a "true" wind direction ϕ_w is obtained by fitting the circle observations to the following expression:

$$\sigma^\circ = B_0 + B_1 \cos 2\phi_0 + B_2 \sin 2\phi_0 \qquad (21)$$

and then

$$\phi_w = \arctan(B_2, B_1)/2 \qquad (22a)$$

or

$$\phi_w = \arctan(B_2, B_1)/2 + 180^\circ. \qquad (22b)$$

The 180° ambiguity is easily resolved by referring to the in situ data that are available for each aircraft mission. The sea surface anemometer observations agree with either (22a) or (22b) to within about 10°. An in situ wind speed measurement is also available.

The observations in each circle dataset are sampled so as to simulate the observations that will be obtained from NSCAT, i.e., three σ° observations with relative azimuth angles of 0°, 20°, and 90°. Three polarization modes are also considered: *VVV*, *VHV*, and *HHH*, where the three letters denote the polarizations for the forward, middle, and aft antennas, respectively. The first two modes will be implemented on NSCAT, but the *HHH* mode will not. For each circle dataset, 36 wind vector retrievals are done for each polarization mode. For example, the first retrieval for the *VVV* mode is done using the *v*-pol NRCS observations for azimuth angles 0°, 20°, and 90°. The next retrieval is done using azimuth angles 10°, 30°, and 100°, and so on. Thus, the 36 retrievals correspond to rotating the wind direction over 360° relative to the NSCAT forward antenna.

For each retrieval, four wind direction ambiguities are found using the two orthogonal observations, as described previously. These ambiguities are then ranked according to the σ° residual S_j given by (20). The Wentz et al. (1986) model is used to specify the A coefficients. Before comparing the retrieved set of wind direction ambiguities to the true wind direction, we merged together those ambiguities that have a directional separation of less than 10°. The purpose of doing this is to reduce the number of ambiguities. The merged ambiguity is found by averaging the two components. The maximum error introduced by this process is 5°, which is within the uncertainty of the retrieval.

Table 2 shows the retrieved wind direction and speed compared to the "true" direction and the in situ speed. In doing these comparisons, we first determine which ambiguity lies closest to the true direction. This ambiguity is called the prime ambiguity. The first two columns in Table 2 show the mean and the standard deviation of the difference in direction between the true vector and the prime ambiguity. These statistics represent 1152 differences (32 circles × 36 wind directions). The mean error is zero, and the standard deviation is about 11°. These statistics are an indication of the accuracy assuming perfect ambiguity selection.

The next three columns relate to ambiguity selection skill. The ambiguities are ranked according to the σ° residual S_j given by (20). The first and second columns

TABLE 2. Statistics on simulated NSCAT wind vector retrieval.

	Direction error (deg)		Ambiguity selection skill			Wind speed error (m s^{-1})	
Mode	Mean	Root-mean-square	Rank 1	Rank 2	Rank >2	Mean	Root-mean-square
VVV	0	11	50%	40%	10%	−3.7	3.8
VHV	0	11	50%	32%	18%	−3.7	3.8
HHH	0	12	56%	35%	9%	−3.3	3.3

show the percentage of occurrences for which the first-ranked and second-ranked ambiguity corresponds to the prime ambiguity. The third column shows the percentage of occurrences for which the prime ambiguity was not the first- or second-ranked ambiguity. For the *VVV* and *HHH* modes, the prime ambiguity is ranked first or second about 90% of the time. The ambiguity selection skill is not as good for the *VHV* mode, where 18% of the time the prime ambiguity is rank 3 or lower.

The comparisons of the prime ambiguity wind speed versus the in situ wind speed show a large discrepancy. The retrieved wind speed is biased about 3.5 m s^{-1} low relative to the in situ values, and the rms variation of the differences is about 3.5 m s^{-1}. This poor agreement is probably due to the large spatial–temporal mismatch between the in situ and aircraft observations, the microscale variability in the wind field, and the absolute calibration error in the scatterometer. The Wentz et al. (1986) model was adjusted to match the Seasat scatterometer observations. Any relative bias between the Seasat scatterometer and the AAFE–RADSCAT scatterometer will introduce a bias in the wind speed retrievals. The wind direction and ambiguity statistics do not require the in situ data, other than resolving the 180° ambiguity in (22).

The statistics on the ambiguity selection skill indicate that it will be difficult, if not impossible, to uniquely determine the wind direction using just NSCAT observations. The first-ranked ambiguity is the correct choice only about 50% of the time. However, one factor working in our favor is that the first- and second-ranked ambiguities are usually vectors pointing in opposite directions. That is to say, the inclusion of a third azimuth look, in general, reduces the ambiguity problem to two possible solutions separated by approximately 180°.

A more meaningful analysis of the scatterometer wind direction skill can be done by assuming there exists some a priori information on the wind direction. For example, a numerical model that is continuously assimilating NSCAT data may be able to forecast the wind direction with an accuracy of ±90°. Then those ambiguities that differ in direction by more than 90° as compared to the predicted direction can be excluded. Under this assumption, the wind vector retrievals are reanalyzed. Those ambiguities for which $|\phi_{wj} - \phi_w|$ exceeds 90° are first excluded, and the remaining ambiguity that has the smallest S_j is selected. The wind direction of the selected ambiguity is then compared with the true direction ϕ_w. The mean difference is 1° and the standard deviation of the difference is 18° for the *VVV* and *HHH* modes and is 24° for the *VHV* mode. The wind speed statistics are the same as shown in Table 2.

The preceding analyses are also done using a least-squares method that searches the wind vector space and finds minima for S_j (Wentz et al. 1982). The results are essentially the same as given by the simpler algorithm, except that the ambiguity selection skill is slightly higher (2%) than the values shown in Table 2.

6. Conclusions

The variation of the sea surface NRCS with the azimuth look angle, as observed by the AAFE–RADSCAT aircraft scatterometer, can be modeled to an accuracy of about 0.5 dB by 1) the traditional second-order harmonic expansion and by 2) the double-cosine function. The quality of fit exhibited by the two forms is essentially the same, considering the variability in the observations. The wind vector retrieval problem is simplified by using the double-cosine function.

The aircraft observations are used as input data to the simplified wind vector retrieval algorithm in order to simulate the operation of NSCAT. For the *VVV* and *HHH* polarization modes, the first- or second-ranked ambiguity is the correct choice 90% of the time. For the *VHV* mode, this skill percentage falls to 82%. This result suggests that the mixing of polarizations may not be desirable for NSCAT.

The first-ranked ambiguity is the correct choice only about 50% of the time. This indicates that it will be difficult, if not impossible, to uniquely determine the wind direction using just NSCAT observations.

Assuming the availability of a priori information that restricts the wind direction to a ±90° range, some ambiguities can be eliminated. The accuracy of the wind direction of the remaining ambiguity with the smallest σ° residual (i.e., first ranked) is 18° for the *VVV* and *HHH* modes and 24° for the *VHV* mode.

There is little difference between the performance of the simplified retrieval algorithm and the more involved least-squares searching algorithm.

Acknowledgments. Funding for this study was provided by Oregon State University under Contract OSU

2-9577-02. This work is part of NASA's NSCAT program.

REFERENCES

Chi, C-Y, and F. K. Li, 1988: A comparative study of several wind estimation algorithms for spaceborne scatterometers. *IEEE Trans. Geosci. Remote Sens.*, **26,** 115–121.

Colton, M. C., 1989: Dependence of radar backscattering on the energetics of the air–sea interface. Ph.D. dissertation, Naval Postgraduate School, Monterey, CA, 319 pp.

Grantham, W. L., E. M. Bracalente, C. L. Britt, F. J. Wentz, W. L. Jones and L. C. Schroeder, 1982: Performance evaluation of an operational spaceborne scatterometer. *IEEE Trans. Geosci. Remote Sens.*, **GE-20,** 250–254.

Jones, W. L., and L. C. Schroeder, 1978: Radar backscatter from the ocean: Dependence on surface friction velocity. *Bound.-Layer Meteor.*, **13,** 133–149.

—— and J. L. Mitchell, 1977: Aircraft measurements of the microwave scattering signature of the ocean. *IEEE J. Oceanic Eng.*, **OE-2,** 52.

——, P. G. Black, D. M. Boggs, E. M. Bracalente, R. A. Brown, G. Dome, J. A. Ernst, I. M. Halberstam, J. E. Overland, S. Peteherych, W. J. Pierson, F. J. Wentz, P. M. Woiceshyn and M. G. Wurtele, 1979: Seasat scatterometer: Results of the Gulf of Alaska workshop. *Science,* **204,** 1413–1415.

——, L. C. Schroeder, D. H. Boggs, E. M. Bracalente, R. A. Brown, G. J. Dome, W. J. Pierson and F. J. Wentz, 1982: The SEASAT-A satellite scatterometer: The geophysical evaluation of remotely sensed wind vectors over the ocean. *J. Geophys. Res.*, **87,** 3297–3317.

Schroeder, L. C., and J. L. Mitchell, 1983: Archival of aircraft scatterometer data from AAFE–RADSCAT Missions. NASA Technical Memo. 84608, 22 pp.

Wentz, F. J., 1979: Design study for future satellite microwave scatterometers. RSS Tech. Rep. 260379, 24 pp. [Remote Sensing Systems, 1101 College Ave, Santa Rosa, CA 95404.]

——, V. J. Cardone and L. S. Fedor, 1982: Intercomparison of wind speeds inferred by SASS, Altimeter, and SMMR. *J. Geophys. Res.*, **87,** 3378–3384.

——, S. Peteherych and L. A. Thomas, 1984: A model function for ocean radar cross sections at 14.6 GHz. *J. Geophys. Res.*, **89,** 3689–3704.

——, L. A. Mattox and S. Peteherych, 1986: New algorithms for microwave measurements of ocean winds: Applications to SEASAT and the Special Sensor Microwave Imager. *J. Geophys. Res.*, **91,** 2289–2307.